LETTER

doi:10.1038/nature10552

Arabian Sea tropical cyclones intensified by emissions of black carbon and other aerosols

Amato T. Evan[1], James P. Kossin[2,3], Chul 'Eddy' Chung[4] & V. Ramanathan[5]

Throughout the year, average sea surface temperatures in the Arabian Sea are warm enough to support the development of tropical cyclones[1], but the atmospheric monsoon circulation and associated strong vertical wind shear limits cyclone development and intensification, only permitting a pre-monsoon and post-monsoon period for cyclogenesis[1–4]. Thus a recent increase in the intensity of tropical cyclones over the northern Indian Ocean[5] is thought to be related to the weakening of the climatological vertical wind shear[3,4]. At the same time, anthropogenic emissions of aerosols have increased sixfold since the 1930s, leading to a weakening of the southwesterly lower-level and easterly upper-level winds that define the monsoonal circulation over the Arabian Sea[6–9]. In principle, this aerosol-driven circulation modification could affect tropical cyclone intensity over the Arabian Sea, but so far no such linkage has been shown. Here we report an increase in the intensity of pre-monsoon Arabian Sea tropical cyclones during the period 1979–2010, and show that this change in storm strength is a consequence of a simultaneous upward trend in anthropogenic black carbon and sulphate emissions. We use a combination of observational, reanalysis and model data to demonstrate that the anomalous circulation, which is radiatively forced by these anthropogenic aerosols, reduces the basin-wide vertical wind shear, creating an environment more favourable for tropical cyclone intensification. Because most Arabian Sea tropical cyclones make landfall[1], our results suggest an additional impact on human health from regional air pollution.

The South Asian atmospheric brown cloud (ABC) is a 3-km-thick layer of pollution over the northern Indian Ocean (NIO) and Indian subcontinent that results from human emission of aerosols such as black and organic carbon and sulfates[9]. When over water the dominant surface-radiative effect of the ABC is a decrease in solar insolation, which is enhanced significantly by black and organic carbon aerosols[7–11]. There is a northward gradient of fine-mode aerosol optical depth over the Arabian Sea (Fig. 1a) and therefore a southward gradient in aerosol surface forcing[7,9,10,12] (that is, negative surface forcing is greater in magnitude to the north). Positive forcing associated with greenhouse gases is offset in the NIO by the sixfold increase in emissions since 1930 (ref. 9), resulting in a southward gradient in sea surface temperature (SST) trends (Fig. 1b) and a decrease in the climatological summertime northward SST gradient[7]. The atmospheric response to this anomalous SST gradient is a weakening of the southerly cross-equatorial surface flow and upper-level tropical easterly jet, which define the Indian monsoon circulation, through anomalously high sea-level pressure to the north and low sea-level pressure to the south[7,8].

Once the monsoon onset occurs, very strong vertical wind shear develops across the Arabian Sea, the main factor prohibiting tropical cyclone development during July and August[1,2]. Thus, despite climatologically warm SST, only two to three tropical cyclones form in the Arabian Sea every calendar year, an average of one storm in the pre-monsoon period (May and June), and one to two storms in the post-monsoon period (August to December)[1].

For a tropical cyclone to intensify, net heat transfer from the ocean to the near-surface air must be sufficient to overcome the frictional drag acting on the cyclone winds in the boundary layer[13]. In the absence of large-scale kinematic forces that would disrupt the physical structure of a cyclone, such as vertical wind shear[14], storm intensity is limited largely by the thermodynamic environment, as described by potential intensity theory[15]. As atmospheric kinematic conditions become more favourable for cyclones to develop, those that do form are more likely to achieve maximum intensities close to their potential intensity. Note that the ABC can affect the mean thermodynamic environment by stabilizing regional atmospheric lapse rates and decreasing potential intensity, but this effect is small relative to the regionally high absolute values of potential intensity[1].

One way to evaluate temporal changes in the intensity of tropical cyclones is to examine cyclone lifetime maximum intensity (LMI), defined as the maximum intensity achieved in the lifetime of a storm[16]. We calculate LMI for each storm from historical estimates of cyclone wind speeds[17] and then separate the data into the 1979–1996 and 1997–2010 periods, because ten pre-monsoon tropical cyclones formed during

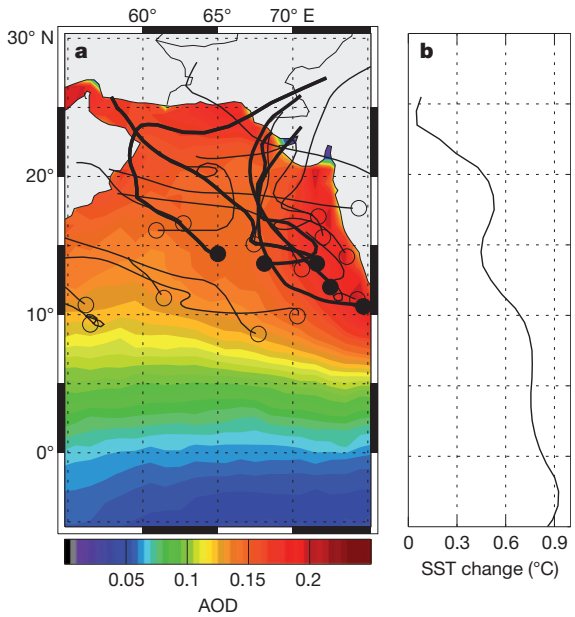

Figure 1 | Tropical cyclone tracks, aerosol optical depth and meridional SST trends in the Arabian Sea. a, Genesis points (circles) and tracks (solid lines) of pre-monsoon tropical cyclones during the period 1979–2010. Storms with an lifetime maximum intensity (LMI) of more than 50 m s^{-1} are indicated with a filled circle at the genesis point and thick track lines. Shaded contours represent annual long-term mean fine-mode aerosol optical depth (AOD) from the MODIS Terra and Aqua instruments averaged over 2003–2009. **b**, The 50-year change in observed SST, averaged over 55°–75° E. The SST change is defined as the average of the monthly linear trend from 1955–2004, multiplied by 50.

[1]University of Virginia, Charlottesville, Virginia 22904, USA. [2]NOAA's National Climatic Data Center, Asheville, North Carolina 28801, USA. [3]NOAA Cooperative Institute for Meteorological Satellite Studies, Madison, Wisconsin 53706, USA. [4]Gwangju Institute of Science and Technology, Gwangju 500712, Republic of Korea. [5]Scripps Institution of Oceanography, University of California at San Diego, La Jolla, California 92093, USA.

each epoch. (At the time of writing, data for the 2010 season were not included in the IBTrACS database; track and intensity data for the 2010 Arabian Sea tropical cyclones are therefore from the 2010 Joint Typhoon Warning Center annual tropical cyclone reports (http://www.usno.navy.mil/JTWC).) The distribution of pre-monsoon LMI shifts substantially towards greater intensity from the early to the later period, whereas the post-monsoon distribution shifts slightly downwards (Fig. 2a). The difference in the pre-monsoon median (and mean) LMI between the periods is significant at greater than the 97% level, but there is no significant statistical separation for the post-monsoon storms.

Arabian Sea tropical cyclone intensity estimates are based on a Dvorak analysis of satellite imagery[18]; given improvements in observational platforms over time it is plausible that the LMI of pre-1998 storms is underestimated, thus causing an apparent increase in the LMI of storms forming after this time. However, if this were true we would expect to see an increase in the LMI of post-monsoon storms, because there is no physical reason why such data artefacts would affect only the pre-monsoon cyclones. Therefore the striking dissimilarity between the changes in distribution of the pre-monsoon and post-monsoon suggests that the change in the pre-monsoon LMI distribution is physical. We repeated this analysis with intensity estimates from an objective analysis of satellite data that is corrected for artefacts related to temporal changes in the observational platform[16,19], obtaining nearly identical results (not shown).

We interpret the increasing LMI of pre-monsoon cyclones as reflecting a more favourable kinematic environment for storms to intensify, especially as a persistently high SST helps to maintain a thermodynamic environment that is favourable for storm intensification[1,3,4]. We speculate that a decrease in the environmental vertical wind shear (defined here as the magnitude of the vector difference between the upper-level and lower-level wind measured along the 200-mbar and 850-mbar pressure levels, respectively) that the storms are experiencing is the catalyst for the increase in pre-monsoon LMI[1,3,4].

Using reanalysis data[20] we test this hypothesis by calculating the storm-ambient vertical wind shear, defined as the vertical wind shear at the location of the storm averaged over the period during which the tropical cyclone's intensity increases from 17 m s^{-1} to its LMI. In a similar manner to a previously described procedure[21], we averaged vertical shear values for every cyclone fix 48 h before the arrival of the storm to decrease contamination of the reanalysis fields by the storms themselves. The distribution of pre-monsoon storm-ambient shear shows a pronounced shift towards lower values from the earlier to the later period (Fig. 2b); the median shear value decreases from 11 to 8 m s^{-1}, and the lower quartile for the earlier period is equal to the upper quartile of the later period.

Models[22] and observations[23] suggest that the relationship between vertical wind shear and tropical cyclone intensity is not linear; rather, a tropical cyclone will tend to weaken or strengthen in the presence of vertical shear that is respectively greater than or less than values within the approximate range 8–11 m s^{-1}. Therefore, as the pre-monsoon shear values become more likely to fall below this range, the storms are more likely to continue intensifying towards their potential intensity and their LMI distribution is expected to shift towards higher values. Although the post-monsoon storm-ambient shear distribution also shifts towards lower values, these values remain mostly within or above this range of thresholds for intensification, and the 1997–2010 post-monsoon shear distribution is not statistically different from the 1979–1996 pre-monsoon shear distribution (Supplementary Table 1). We repeated this analysis using two additional data sets (Supplementary Figs 3–5), obtaining quantitatively similar results (Supplementary Table 1).

We propose that this change in storm-ambient shear is related to a broader downward trend in regional vertical wind shear that results from a simultaneous increase in regional anthropogenic emissions of aerosols. Observational evidence demonstrates that the ABC leads to widespread surface solar dimming of the order of 15–20 W m^{-2} over the Arabian sea during the pre-monsoon months[10], and trend analyses of surface solar radiation observations by broad band solar radiometers[9,24] reveal a nearly 20 W m^{-2} decrease in surface solar radiation from 1950 to 2000, roughly 10% of the climatological solar radiation absorbed at the surface. The dimming is accompanied by a large solar heating of the atmosphere, thus stabilizing the column and further exacerbating the weakening of the circulation resulting from the dimming[9]. We quantify the influence of ABC surface and atmospheric radiative forcing on vertical wind shear by means of numerical experiments designed to identify the response of the regional circulation to the increasing emissions of aerosols over the period 1950–2000 (model experiment details are in Methods).

We estimate the 30-year change in observed pre-monsoon SST by multiplying by 30 the averaged linear trend of observed May and June monthly mean SST[25] over the period 1979–2010. To facilitate comparison of SST between the model output and observations we subtract from the observed 30-year SST change the equatorial mean (5° S to 5° N and 55° E to 75° E) 30-year change in SST of 0.3 °C (Fig. 3a). We interpret this equatorial change in observed SST as reflecting positive forcing from greenhouse gases. The anomalous 30-year SST change from the model experiments is obtained by differencing the May and June ensemble mean of the perturbation and control experiments. Because the model experiments reflect the SST change from the growth of the optical depth of the ABC over the 50-year period 1950–2000, we assume a linearized response of SST to ABC radiative forcing and scale the model results by three-fifths to estimate the SST change from a 30-year increase in the optical depth of the ABC (Fig. 3b). The observed and modelled southward gradients of the 30-year SST change are

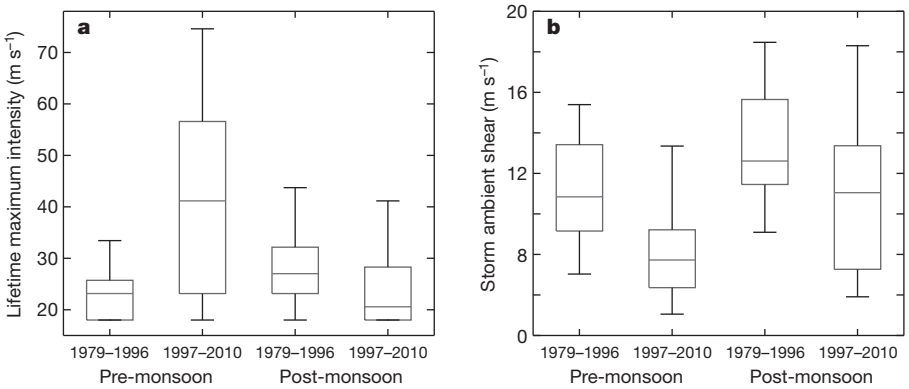

Figure 2 | Distributions of pre-monsoon and post-monsoon LMI and storm-ambient vertical wind shear. Box plots of LMI (**a**) and storm-ambient vertical wind shear (**b**) showing the medians (central lines), inner quartile ranges (boxes), and the 25th and 75th centiles minus and plus 1.5 times the inner quartile range, respectively (whiskers). Shear is calculated from the National Center for Environmental Prediction-Department of Energy Reanalysis[20]. The significance of the separation of the median and mean values is given in Supplementary Table 1.

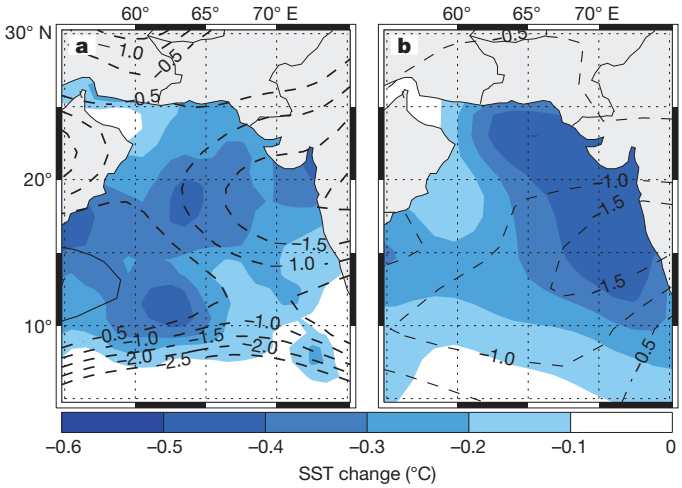

Figure 3 | Thirty-year trends in pre-monsoon SST and vertical wind shear. The 30-year trends in vertical wind shear (contours) based on reanalysis data from 1979–2010 (**a**) and numerical experiments designed to isolate the effect of the ABC on the regional circulation[7] (**b**). Dashed contours indicate negative trends, and solid contours indicate positive trends; the zero contour is not shown. Positive and negative shear contours are in units of 0.5 m s^{-1}. Shading shows the 30-year SST trends over the same period from observations (**a**), which is relative to the equatorial SST trend, and the aerosol-forced SST change prescribed in the model experiments (**b**).

similar in magnitude, with SST warming at 5° N being 0.5 °C greater than the warming at 15° N in both.

We estimate the historical 30-year change in pre-monsoon vertical wind shear by multiplying by 30 the averaged May and June linear trend of vertical shear from reanalysis[20] (Fig. 3a). We assume a linear response of the atmosphere to growth of the ABC and estimate the ABC-forced 30-year change in pre-monsoon vertical wind shear as the difference in ensemble mean May and June vertical shear, scaled by three-fifths (Fig. 3b). The reanalysis and modelled 30-year change in pre-monsoon vertical wind shear are in good agreement north of 10° N, where the ABC is present and where most pre-monsoon Arabian Sea tropical cyclones form and track (Fig. 1a). Each data point shows a 1.5 m s^{-1} decrease off the western coast of the Indian subcontinent, and northward and westward from this location the change in shear in each is 1.0 m s^{-1}. This agreement is compelling evidence that the basin-wide decrease in vertical wind shear is causally related to the increasing intensity of the ABC. We compared the model output with trends in vertical shear from two additional reanalysis data sets, obtaining nearly identical results (Supplementary Fig. 6).

Noting that the distribution of post-monsoon storm-ambient shear and LMI during the 1997–2010 period is similar to those pre-monsoon distributions for the 1979–1996 time span (Fig. 2 and Supplementary Table 1), it can be argued that a further decrease in basin-wide shear associated with projected growth in emissions[9] will further shift the inner quartile range of the post-monsoon storm-ambient shear distribution towards that of the pre-monsoon shear during the latter period. In such a case it is plausible that very intense tropical cyclones, which have so far been limited to the pre-monsoon period, could begin to emerge in the post-monsoon season as well.

Given the relatively small size of the Arabian basin, more than half of all cyclones that form here make landfall, and even weak landfalling Arabian Sea cyclones can cause considerable destruction and loss of life[1] (see also the Joint Typhoon Warning Center annual tropical cyclone reports, and the EM-DAT International Disaster Database (http://www.emdat.be/disaster-list)). All of the most powerful cyclones in the Arabian Sea that occurred during the past 30 years formed during the pre-monsoon period and made landfall in India, Pakistan, Oman or Iran, causing considerable loss of life and substantial damage (Table 1). In addition to the multitude of known human health impacts associated with aerosols that comprise the ABC[26], we suggest that the increasing intensity of landfalling tropical cyclones is a consequence of regional emissions of pollution aerosols. Because tropospheric aerosols have a short residence time, decreasing emissions should have a nearly immediate effect on the propensity of pre-monsoon tropical cyclones to reach their maximum potential intensity. However, we caution that this study is conducted from a limited sample of storms; continued research that tests the relationship between aerosols and tropical cyclones in the NIO is warranted.

METHODS SUMMARY

The numerical experiments used here are identical to those described previously[7], and we refer the reader to that paper and the online Methods for a detailed discussion of the model setup. These experiments were performed using an atmospheric general circulation model[27]. In the control and perturbation experiments an SST annual cycle is prescribed. In the control experiment SST is prescribed as observed mean SST[25] changes from 1950 to 2000. In the perturbation experiment SST in the NIO is estimated to be the equivalent 50-year change in SST assuming that regional emissions had been stabilized at 1950s levels, so that SST is everywhere the same as in the control experiment, except in the NIO, where the local 50-year SST change is forced to be equal to the SST change in the equatorial Indian Ocean[9]. SST in the NIO is warmer in the perturbation run than it is in the control run, and the difference in the zonally averaged (Indian Ocean) meridional SST gradient in the experiments is nearly identical to that from Fig. 1b, except that in the model the difference is zero at the Equator and negative to the north. The perturbation experiment also includes the seasonally varying effect of heating in the atmosphere by the ABC[28]. We interpret the difference between the 50-member ensemble mean of the control and perturbation experiments as the influence of the 50-year growth in regional emissions on the atmospheric circulation.

Full Methods and any associated references are available in the online version of the paper at www.nature.com/nature.

Received 20 May; accepted 7 September 2011.

1. Evan, A. T. & Camargo, S. J. A climatology of Arabian Sea cyclonic storms. *J. Clim.* **24,** 140–158 (2011).
2. Gray, W. M. Global view of the origin of tropical disturbances and storms. *Mon. Weath. Rev.* **96,** 669–700 (1968).
3. Krishna, K. M. Intensifying tropical cyclones over the North Indian Ocean during summer monsoon—global warming. *Global Planet. Change* **65,** 1–2,–12–16 (2009).
4. Rao, V. B., Ferreira, C. C., Franchito, S. H. & Ramakrishna, S. S. V. S. In a changing climate weakening tropical easterly jet induces more violent tropical storms over the north Indian Ocean. *Geophys. Res. Lett.* **35,** L15710 (2008).
5. Singh, O. P., Kahn, A. & Rahman, S. Has the frequency of intense tropical cyclones increased in the North Indian Ocean? *Curr. Sci.* **80,** 575–580 (2001).
6. Dash, S. K., Kulkarni, M. A., Mohanty, U. C. & Prasad, K. Changes in the characteristics of rain events in India. *J. Geophys. Res.* **114,** D10109 (2009).
7. Chung, C. E. & Ramanathan, V. Weakening of North Indian SST gradients and the monsoon rainfall in India and the Sahel. *J. Clim.* **19,** 2036–2045 (2006).

Table 1 | Characteristics of the five most powerful Arabian Sea tropical cyclones, 1980–2010

Cyclone name	Year	LMI (m s^{-1})	Landfall location	Lives lost	Number of people affected	Damage (×10^6 2011 US$)
03A	1998	54	Gujarat, India	2,871	2,871	643
02A	1999	57	Karachi, Pakistan	682	576,636	42
01A	2001	57	Gujarat, India	None	None	None
Gonu	2007	75	Muscat, Oman; Ras Al Kuh, Iran	88	180,009	4,203
Phet	2010	64	Muscat, Oman; Karachi, Pakistan	39	4,000	1,845

Data are shown for the five most powerful Arabian Sea cyclones between 1980 and 2010, all of which formed during the pre-monsoon period. Landfall locations, fatalities, numbers affected and damage data are from the Joint Typhoon Warning Center's annual tropical cyclone reports and the EM-DAT International Disaster Database.

8. Meehl, G., Arblaster, J. & Collins, W. Effects of black carbon aerosols on the Indian monsoon. *J. Clim.* **21,** 2869–2882 (2008).
9. Ramanathan, V. *et al.* Atmospheric brown clouds: impacts on South Asian climate and hydrological cycle. *Proc. Natl Acad. Sci. USA* **102,** 5326–5333 (2005).
10. Ramanathan, V. *et al.* The Indian Ocean experiment: an integrated assessment of the climate forcing and effects of the great Indo-Asian haze. *J. Geophys. Res.* **106,** 28371–28398 (2001).
11. Wang, C., Kim, D., Ekman, A. M. L., Barth, M. C. & Rasch, P. J. Impact of anthropogenic aerosols on Indian summer monsoon. *Geophys. Res. Lett.* **36,** L21704 (2009).
12. Chung, C. E., Ramanathan, V., Kim, D. & Podgorny, I. Global anthropogenic aerosol direct forcing derived from satellite and ground-based observations. *J. Geophys. Res.* **110,** D24207 (2005).
13. Emanuel, K. Tropical cyclones. *Annu. Rev. Earth Planet. Sci.* **31,** 75–104 (2003).
14. DeMaria, M. & Kaplan, J. An updated statistical hurricane intensity prediction scheme (SHIPS) for the Atlantic and eastern North Pacific basins. *Weather Forecast.* **14,** 326–337 (1999).
15. Emanuel, K. A. The maximum intensity of hurricanes. *J. Atmos. Sci.* **45,** 1143–1155 (1988).
16. Elsner, J. B., Kossin, J. P. & Jagger, T. H. The increasing intensity of the strongest tropical cyclones. *Nature* **455,** 92–95 (2008).
17. Knapp, K. P., Kruk, M. C., Levinson, D. H., Diamond, H. J. & Neumann, C. J. The International Best Track Archive for Climate Stewardship (IBTrACS): unifying tropical cyclone data. *Bull. Am. Meteorol. Soc.* **91,** 363–376 (2010).
18. Dvorak, V. F. *Tropical Cyclone Intensity Analysis using Satellite Data.* Technical Report no. 11 (NOAA, 1984).
19. Kossin, J. P., Knapp, K. R., Vimont, D. J., Murnane, R. J. & Harper, B. A. A globally consistent reanalysis of hurricane variability and trends. *Geophys. Res. Lett.* **34,** L04815 (2007).
20. Kanamitsu, M. *et al.* NCEP-DOE AMIP-II reanalysis (R-2). *Bull. Am. Meteorol. Soc.* **83,** 1631–1643 (2002).
21. Kossin, J. P. & Camargo, S. J. Hurricane track variability and secular potential intensity trends. *Clim. Change* **97,** 329–337 (2009).
22. Frank, W. M. & Ritchie, E. A. Effects of vertical wind shear on the intensity and structure of numerically simulated hurricanes. *Mon. Weath. Rev.* **129,** 2249–2269 (2001).
23. Elsberry, R. L. & Jeffries, R. A. Vertical wind shear influences on tropical cyclone formation and intensification during TCM-92 and TCM-93. *Mon. Weath. Rev.* **124,** 1374–1387 (1996).
24. Kumari, P. B., Londhe, A. L., Daniel, S. & Jadhav, D. B. Observational evidence of solar dimming: offsetting surface warming over India. *Geophys. Res. Lett.* **34,** L21810 (2007).
25. Rayner, N. A. *et al.* Global analyses of sea surface temperature, sea ice, and night marine air temperature since the late nineteenth century. *J. Geophys. Res.* **108,** 4407 (2003).
26. UNEP. *Integrated Assessment of Black Carbon and Tropospheric Ozone - Summary for Decision Makers.* UNEP/GC/26/INF/20 (United Nations Environment Program and World Meteorological Organization, 2011).
27. Kiehl, J. T. *et al.* The National Center for Atmospheric Research Community Climate Model: CCM3. *J. Clim.* **11,** 1131–1149 (1998).
28. Chung, C. E. & Ramanathan, V. South Asian haze forcing: remote impacts with implications to ENSO and AO. *J. Clim.* **16,** 1791–1806 (2003).

Supplementary Information is linked to the online version of the paper at www.nature.com/nature.

Acknowledgements Partial funding for this work was provided by National Oceanic & Atmospheric Administration (NOAA)/Climate Program Office (NA10OAR4310136), Korea's Research Agency for Climate Science (RACS 2010-2603) and the National Science Foundation (ATM-0721142). Data from National Centers for Environmental Prediction reanalyses 1 and 2 were provided by the NOAA/Office of Oceanic and Atmospheric Research/Earth System Research Laboratory Physical Sciences Division, Boulder, Colorado, USA, from their website (http://www.esrl.noaa.gov/psd/).

Author Contributions A.E. and V.R. conceived the project. A.E. and J.K. designed the study. A.E., J.K. and E.C. provided model and observational data. All authors participated in data interpretation and co-wrote the manuscript.

Author Information Reprints and permissions information is available at www.nature.com/reprints. The authors declare no competing financial interests. Readers are welcome to comment on the online version of this article at www.nature.com/nature. Correspondence and requests for materials should be addressed to A.E. (ate9c@virginia.edu).

METHODS

The numerical experiments used in this study to identify the effect of increasing emissions on vertical wind shear are identical to those described previously[7], and we refer the reader to that paper for a comprehensive discussion of the experimental setup and model results. These numerical experiments were performed with the National Center for Atmospheric Research Community Climate Model Version 3 (NCAR/CCM3)[27] at a T42/L18 resolution with prescribed SST. For each of the control and perturbation experiments there were ten ensemble member simulations, all ten with different initial conditions. For each of the ten ensemble simulations the model was spun up to equilibrium for one year, and then run for an additional five years. The ten 5-year simulations were averaged, yielding a 50-year sample for each of the ensemble means considered here.

In the control run and perturbation run, an SST annual cycle is prescribed. In the control experiment, SST is prescribed to globally reflect observed long-term SST[25] changes from 1950 to 2000. This is achieved by calculating the monthly linear SST trend over the period 1951–2002, multiplying the trend by 50 (°C per 50 years), and adding this 50-year SST change to the observed monthly SST climatology (calculated over the period 1951–2002). Therefore, in the control experiment, SST in the NIO reflects a 50-year increase in emissions and negative surface forcing by the ABC. In the perturbation experiment, SST in the NIO is estimated to be the equivalent 50-year change in SST assuming that regional emissions had been stabilized at 1950s levels, such that SST is everywhere the same as in the control experiment, except in the NIO, where the local 50-year SST change is forced to be equal to the SST change in the equatorial Indian Ocean, consistent with previous findings[9].

SST in the NIO is warmer in the perturbation run than it is in the control run, and the difference in the zonally averaged (Indian Ocean) meridional SST gradient in the experiments is nearly identical to that from Fig. 1b, except that in the model the difference is zero at the Equator and negative to the north. This difference in SST is equivalent to the radiatively forced change in SST from the increase in emissions over the same 50-year period, as demonstrated previously[10]. The perturbation experiment also includes the effect of heating in the atmosphere by the absorption of short-wave and long-wave radiation by the ABC; consistent with ref. 28, a decrease in surface solar insolation was prescribed, as was atmospheric heating from the surface boundary layer to a height of roughly 3 km. The seasonality of the surface forcing and imposed heating is consistent with that of the ABC[9]. We interpret the difference between the ensemble mean of the control and perturbation experiments as being the influence of the 50-year growth in regional emissions on the atmospheric circulation.